

Magnetic-field Induced Topological Transitions and Thermal Conductivity in a Generalized Kitaev Model

Heqiu Li,¹ Yong Baek Kim,^{1,2,*} and Hae-Young Kee^{1,3,†}

¹Department of Physics, University of Toronto, Toronto, Ontario M5S 1A7, Canada

²School of Physics, Korea Institute for Advanced Study, Seoul 02455, Korea

³Canadian Institute for Advanced Research, CIFAR Program in Quantum Materials, Toronto, Ontario M5G 1M1, Canada

(Dated: June 30, 2022)

Recent experiments on Kitaev spin liquid candidate materials reported non-monotonic behavior of thermal conductivity as a function of magnetic field, which lead to conflicting interpretations of its origin. Motivated by this development, we study the magnetic field dependence of thermal conductivity of a generalized Kitaev model, which allows the phase transitions between different flux sectors as a function of the magnetic field. The thermal conductivity due to Majorana fermions shows dip-bump structures as the magnetic field increases, which is caused by either the transitions between different flux sectors of Kitaev spin liquids or the topological transitions that change the Majorana Chern number within the same flux sector. It is shown that the change of Chern number is closely related to the four-Majorana-fermion interaction induced by the magnetic field. The non-monotonic behavior in thermal conductivity emerges at finite temperature, and it becomes weaker when temperature decreases toward zero. Our model provides a generic mechanism for the Kitaev spin liquids to develop non-monotonic magnetic-field dependence of thermal conductivity while the comparison to realistic materials remains an open question for future investigation.

I. INTRODUCTION

Quantum spin liquid is an exotic phase of quantum magnets that has drawn great attention since it was initially proposed¹. Contrary to conventional magnetic phases, quantum spin liquids are not magnetically ordered down to zero temperature, and the spins are fractionalized into spinon quasi-particles coupling to emergent gauge fields, exhibiting a lot of interesting collective phenomena including fractionalized excitations, ground state degeneracy and long range entanglement^{2–8}. The celebrated Kitaev honeycomb model⁹ is exactly solvable with quantum spin liquid ground state. Kitaev spin liquids arise from the bond-dependent spin interactions that frustrate the spin orientation at each site, which can be generated from t_{2g} orbitals with $j_{\text{eff}} = \frac{1}{2}$ in materials with strong spin-orbit coupling¹⁰. The Kitaev honeycomb model provides a plausible platform for the experimental realization of quantum spin liquid, which leads to significant experimental and theoretical efforts in studying Kitaev materials^{10–22}, and many Kitaev spin liquid candidates including $(\text{Na,Li})_2\text{IrO}_3$ ^{23–29} and $\alpha\text{-RuCl}_3$ ^{30–38} are identified.

Recent thermal transport experiments on Kitaev spin liquid candidate $\alpha\text{-RuCl}_3$ have reported non-monotonic dependence of longitudinal thermal conductivity on magnetic field similar to quantum oscillations^{39,40}. There exist several explanations for the reason of this non-monotonic behavior, e.g., from the quantum oscillation from spinon Fermi surface³⁹ or from phase transitions in the spin liquid^{40,41}. Contrary to ordinary quantum oscillations in fermionic systems which arise from quantized Landau levels, the spinons in quantum spin liquids are charge neutral and they cannot directly couple to orbital magnetic field to give Landau levels. Therefore, the mechanism of this non-monotonic behavior in thermal conductivity remains an open question.

Motivated by these experiments, in this work we explore what mechanism can lead to non-monotonic dips and bumps

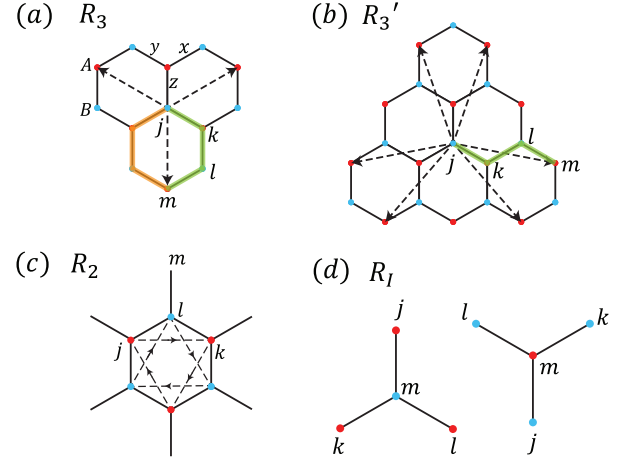


FIG. 1. Illustration of terms in the Hamiltonian. A and B sublattices are labeled as red and blue dots. The dashed arrows in (a),(b),(c) represent R_3 , R_3' and R_2 respectively. (d) shows the relative locations of the sites in R_1 . The sites at A and B sublattices are labeled by red and blue dots.

in thermal conductivity as a function of magnetic field. We consider a generalized Kitaev model and demonstrate that dips and bumps in thermal conductivity can arise naturally due to phase transitions induced by the magnetic field. Two important ingredients are included in this generalized Kitaev model, the frustrated further-neighbour Majorana hopping from spin interactions^{42,43} and the four-Majorana interaction induced by the magnetic field.

The frustrated further-neighbour Majorana hopping allows different flux sectors to be the ground state. In Kitaev spin liquids spinons are coupled to an emergent \mathbb{Z}_2 gauge field and each plaquette can have \mathbb{Z}_2 flux 0 or π , where π flux corresponds to a vison. Based on the density and distribution of

visions, the quantum spin liquid can be classified into different flux sectors. Each flux sector has distinct spinon spectrum and free energy. The original Kitaev honeycomb model has its ground state in the 0-flux sector where all plaquettes have 0 flux by Lieb's theorem⁴⁴. If further-neighbour Kitaev spin interactions are considered, frustrated third neighbour Majorana hopping terms^{42,43} can arise. These terms commute with the \mathbb{Z}_2 gauge field hence they preserve the exact-solubility of the model. With these terms, different flux sectors can be stabilized as the ground state, which opens up the possibility for phase transitions between flux sectors. The magnetic field perturbatively generates both Majorana hopping terms and four-Majorana interaction terms. We consider both types of terms and applied self-consistent mean field theory to decouple the Majorana interaction. We found that the Majorana interaction can effectively rescale the frustrated hopping and lead to transitions that can change Majorana Chern number.

We take into account these frustrated hopping terms and the four-Majorana interaction in the generalized Kitaev model. We show that external magnetic field can lead to transitions between different flux sectors as well as topological transitions within each flux sector that change the Majorana Chern number. Because different flux sectors have distinct spinon spectrum and thermal conductivity, and because thermal conductivity is sensitive to the spinon band gap which must close when Chern number changes, these phase transitions will lead to dips and bumps in thermal conductivity as a function of magnetic field.

This paper is organized as follows. In Section II we establish the generalized Kitaev model that includes the four-Majorana interaction terms induced by magnetic field and the frustrated Majorana hopping terms. In Section III we utilize self-consistent mean field theory to compute Majorana interaction. In Section IV we present our computation of thermal conductivity and show that it is a non-monotonic function of magnetic field with dips and bumps. In Section V we show that this dip-bump feature in thermal conductivity originates from phase transitions induced by magnetic field. Further relation between our results and the experiments are discussed in the discussion section.

II. GENERALIZED KITAEV MODEL WITH MULTIPLE FLUX SECTORS

The Hamiltonian of the original Kitaev honeycomb model⁹ with nearest neighbour (NN) spin interactions is given by

$$H_1 = -K_1 \sum_{\langle jk \rangle} \sigma_j^\alpha \sigma_k^\alpha = iK_1 \sum_{\langle jk \rangle} u_{jk} c_j c_k, \quad (1)$$

where j, k denote lattice sites, the spin operator at each site is represented by $\sigma_j^\alpha = ib_j^\alpha c_j$, and the \mathbb{Z}_2 gauge field $u_{jk} = ib_j^\alpha b_k^\alpha$ where $\alpha \in \{x, y, z\}$ is fixed by the direction of bond jk . We choose the gauge such that in the 0-flux sector $u_{jk} = +1$ if j (k) is at A (B) sublattice, where A, B sublattices are labeled in Fig.1 (a). The original Kitaev model H_1 considers nearest neighbour interaction and the ground state is in the 0-flux

sector. In real materials, further-neighbour spin interactions exist in general. These longer-range interactions are allowed by symmetry, and they can stabilize different flux sectors as the ground state and lead to phase transitions between different flux sectors. Therefore, we consider a generalized Kitaev model with additional third-neighbour spin interaction terms proposed in Refs 42 and 43:

$$H_3 = K_3 \sum_{\langle jklm \rangle \in R_3} \sigma_j^\alpha \sigma_k^\gamma \sigma_l^\alpha \sigma_m^\gamma - K'_3 \sum_{\langle jklm \rangle \in R'_3} \sigma_j^\alpha \sigma_k^\beta \sigma_l^\beta \sigma_m^\alpha \quad (2)$$

Here R_3 and R'_3 denote the sets of vectors shown in Fig.1 (a) and (b) respectively, and $\langle jklm \rangle \in R_3$ means the sites j and m are connected by the zigzag line passing through jk and lm with $\mathbf{r}_m - \mathbf{r}_j \in R_3$. The summation is over all such zigzag lines. α is along the direction of bond jk , γ is along bond lm , and β is distinct from the directions of jk and kl . In terms of Majorana fermions, H_3 can be rewritten as

$$H_3 = -iK_3 \sum_{\langle jklm \rangle \in R_3} u_{jk} u_{kl} u_{lm} c_j c_m - iK'_3 \sum_{\langle jklm \rangle \in R'_3} u_{jk} u_{kl} u_{lm} c_j c_m$$

These terms commute with gauge field u_{jk} , hence they preserve the exact solubility of the model and the ground state can still be labeled by flux sectors as the original Kitaev model. Note that each vector in R_3 corresponds to two zigzag lines (marked by colors in Fig.1 (a)), and the contribution from these two paths will cancel out if there is a π -flux inside the hexagon. Hence the π -flux sector in which every hexagon has flux π is not affected by the K_3 term. It has been shown that by varying K_3 and K'_3 , different flux sectors can be stabilized as the ground state^{42,43}.

The external magnetic field can generate three-spin interactions in the Kitaev model as follows⁹:

$$H_h = -h \sum_{\langle jlk \rangle \in R_2} \sigma_j^\alpha \sigma_k^\beta \sigma_l^\gamma - h \sum_{\langle jlk \rangle \in R_I} \sigma_j^\alpha \sigma_k^\beta \sigma_l^\gamma \quad (3)$$

Here R_2 and R_I are shown in Fig.1 (c) and (d) respectively. The choice of α, β, γ for the first term is along jl, lk, lm respectively and for the second term is along jm, km, lm respectively. These terms arise from the leading order perturbation of magnetic field and $h \sim \frac{B_x B_y B_z}{K_1^2}$. When these terms are rewritten as Majorana fermions, the first term becomes a NNN hopping term and the second term becomes a four-Majorana interaction term:

$$H_h = H_2 + H_I, \quad H_2 = -ih \sum_{\langle jlk \rangle \in R_2} u_{jl} u_{lk} c_j c_k \quad (4)$$

$$H_I = -h \sum_{\gamma} u_{jm} u_{km} u_{lm} c_m c_j c_k c_l - h \sum_{\lambda} u_{jm} u_{km} u_{lm} c_m c_j c_k c_l \quad (5)$$

Here the relative locations of sites in H_I are shown in Fig.1(d). The total Hamiltonian for the generalized Kitaev model is

$$H = H_1 + H_2 + H_3 + H_I \quad (6)$$

This Hamiltonian is symmetric under space-inversion and threefold rotation. It also has a gauge symmetry indicated by $c_j \rightarrow (-1)^{n_j} c_j$, $u_{jk} \rightarrow (-1)^{n_j - n_k} u_{jk}$ where $n_j \in \{0, 1\}$. Time-reversal maps $h \sim \frac{B_x B_y B_z}{K_1^2}$ to $-h$, hence time-reversal symmetry is broken by H_2 and H_I terms induced by the magnetic field. Without the magnetic field, the Hamiltonian describes a system of free Majorana fermions for each given flux sector, and different flux sectors can be stabilized as the ground state when we vary parameters K_3 and K'_3 . The magnetic field breaks time-reversal symmetry and brings in interactions between Majorana fermions. We show below that the magnetic field can induce first-order transitions between different flux sectors, and within the same flux sector the increasing magnetic field can also induce topological transitions that changes the Chern number of occupied bands. Both effects can lead to jumps and bumps in physical observables including thermal conductivity.

III. MEAN FIELD THEORY FOR MAJORANA INTERACTIONS

We handle the four-Majorana interactions H_I in Eq.(5) by self-consistent mean field theory. For each flux sector, H_I contains terms like $\pm |h| c_m c_j c_k c_l$. Denote the center of each λ or γ by site m . Note that $\pm |h| c_m c_j c_k c_l = -\frac{|h|}{2} (\pm i c_m c_j + i c_k c_l)^2 + |h|$, we can make a Hubbard-Stratonovich (H-S) transformation to decouple the square term. To preserve the threefold rotational symmetry we introduce three real auxiliary fields $\Delta_{jk}, \Delta_{kl}, \Delta_{lj}$. Define $\eta_{mjkl} = -\text{sign}(h) u_{jm} u_{km} u_{lm} = \pm 1$, then the H-S transformation is given by:

$$\begin{aligned} & -h u_{jm} u_{km} u_{lm} c_m c_j c_k c_l = |h| \eta_{mjkl} c_m c_j c_k c_l \\ & \rightarrow \frac{3\Delta_{kl}^2}{2|h|} - i\Delta_{kl}(\eta_{mjkl} c_m c_j + c_k c_l) \\ & + \frac{3\Delta_{lj}^2}{2|h|} - i\Delta_{lj}(\eta_{mjkl} c_m c_k + c_l c_j) \\ & + \frac{3\Delta_{jk}^2}{2|h|} - i\Delta_{jk}(\eta_{mjkl} c_m c_l + c_j c_k) + |h| \end{aligned} \quad (7)$$

Here the factor of 3 is to ensure integrating out the Δ 's recovers the original four-fermion interaction, and η_{mjkl} keeps track of the overall sign of the four-Majorana term. We apply Eq.(7) to H_I with distinct Δ 's for each term, then we have decoupled the Majorana interaction into free Majorana coupled to auxiliary fields. We further require the terms related by a translation of (extended) lattice vector have the same Δ , then the decoupling preserves the translational symmetry. The number of independent Δ 's is three times the number of sites in the extended unit cell for each flux sector. For example, the 0-flux sector has two sites in the unit cell and it needs six Δ 's. The π -flux sector is shown in Fig.2(a), where the signs of the \mathbb{Z}_2 gauge field u_{jk}

at the thick black bonds are flipped. The extended unit cell of the π -flux sector has four sites and it needs twelve Δ 's.

The mean field solution is obtained by finding the set of Δ 's that minimizes the free energy. This is also equivalent to finding Δ 's that satisfy the self-consistency equations:

$$\begin{aligned} \Delta_{kl} &= \frac{|h|}{3} \langle i\eta_{mjkl} c_m c_j + i c_k c_l \rangle \\ \Delta_{lj} &= \frac{|h|}{3} \langle i\eta_{mjkl} c_m c_k + i c_l c_j \rangle \\ \Delta_{jk} &= \frac{|h|}{3} \langle i\eta_{mjkl} c_m c_l + i c_j c_k \rangle \end{aligned} \quad (8)$$

Here the average denotes the thermal average at the same temperature as the temperature under which the free energy is computed. It is evident from Eq.(8) that the Δ 's are real. Our mean field theory is different from Ref 45 in that our decoupling ensures the mean field solution obtained by solving the self-consistency equations and minimizing free energy agree with each other. We have computed the mean field solutions for different flux sectors with flux $0, \pi, \frac{1}{2}\pi, \frac{1}{3}\pi, \frac{2}{3}\pi, \frac{1}{4}\pi, \frac{3}{4}\pi$.

Our solutions show that the Δ 's respect the symmetries of each flux sector. For example, the 0-flux sector has uniform flux distribution in space, and all the Δ 's in Eq.(7) have the same magnitude in the mean field solution. We can label each Δ term by a colored bond with half the length of a NN bond as in Fig.2(c). The sign of Δ 's are distributed in such a way that it modifies the NN hopping strength from K_1 to $K_1 + 2\Delta$, where the factor of 2 is because each NN bond is shared by two Δ 's as in Fig.2(c), and the NNN hopping strength is modified from h to $h + \Delta$. The uniform magnitude of Δ 's also appears in the π -flux sector. For other flux sectors whose flux distribution in space is not uniform, e.g., the $\frac{1}{4}\pi$ -flux phase in Fig.2(b), only the symmetry-related Δ 's have the same magnitude. Here all the Δ 's at the blue bonds in Fig.2(b) have the same value Δ_a , and all Δ 's at the red bonds have another value Δ_b . As the magnetic field increases, Δ also increases and the ratio Δ/h becomes a constant at large h , as shown Fig.2(d). With this mean field solution, we are able to compute the Majorana spectrum and the evolution of thermal conductivity with magnetic field.

IV. THERMAL CONDUCTIVITY

Thermal conductivity can be computed from the mean field Hamiltonian for each flux sector. The Hamiltonian in momentum space is $H = \sum_{\mathbf{k}} \psi_{\mathbf{k},i}^\dagger H^\Delta(\mathbf{k})_{ij} \psi_{\mathbf{k},j}$, where $\psi_{\mathbf{k},j} = \frac{1}{\sqrt{2N}} \sum_j e^{i\mathbf{k}\cdot\mathbf{r}_j} c_j$ is the Fourier transform of Majorana operators, $H^\Delta(\mathbf{k})$ is the Hamiltonian matrix that also depends on Δ 's. The system has zero chemical potential, and the heat current operator is given by⁴⁶

$$\mathbf{J}^Q = \sum_{\mathbf{k}} \psi_{\mathbf{k},i}^\dagger \left(\frac{1}{2} \partial_{\mathbf{k}} (H^\Delta(\mathbf{k})^2) \right)_{ij} \psi_{\mathbf{k},j} \quad (9)$$

The current-current correlation in Matsubara frequency is

$$\Pi_{\mu\nu}(i\Omega_n) = - \int_0^\beta d\tau e^{i\Omega_n \tau} \langle T_\tau J_\mu^Q(\tau) J_\nu^Q(0) \rangle \quad (10)$$

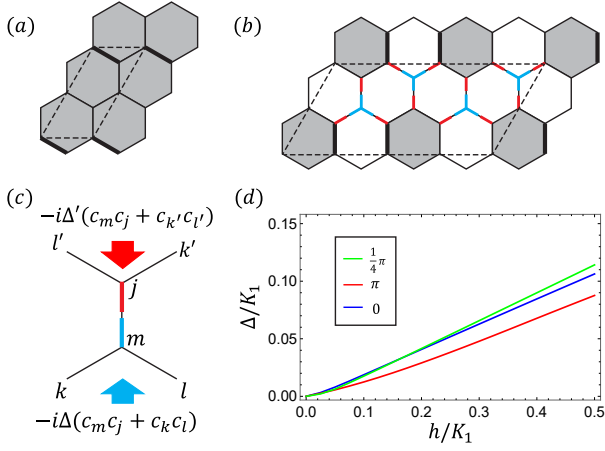


FIG. 2. (a): π -flux sector in which every hexagon has flux π . The \mathbb{Z}_2 gauge field u_{jk} flips sign at the thick black bonds to give rise to π flux in the hexagons near it. The extended unit cell is denoted by the parallelogram. (b): $\frac{1}{4}\pi$ -flux sector where white(gray) hexagons have $0(\pi)$ flux inside it. u_{jk} flips sign at the thick black bonds. The extended unit cell is denoted by the parallelogram. In the mean field solution all the Δ 's labeled by the blue (red) bonds have the same magnitude, which preserves the symmetry of the flux sector. (c): Different terms in the mean field Hamiltonian with Δ and Δ' are labeled by blue and red bonds respectively. (d): Δ as a function of h for 0-, π - and $\frac{1}{4}\pi$ -flux sectors computed at $K_1 = 1, K_3 = 0.3, K'_3 = 0.34, T = \frac{1}{24}$. For $\frac{1}{4}\pi$ -flux sector the Δ at the blue bonds in (b) are used. Δ increases with h as magnetic field increases, and the Δ becomes linear in h when h is large.

The thermal conductivity κ_{xx} can be computed by^{47–49}

$$\begin{aligned} \kappa_{xx} &= -\lim_{\Omega \rightarrow 0} \frac{\text{Im} \Pi_{xx}(\Omega + i\delta)}{\Omega T} \\ &= \lim_{\Omega \rightarrow 0} \pi \int \frac{d^2 k}{(2\pi)^2} \int_{-\infty}^{\infty} d\omega \frac{n_F(\omega) - n_F(\omega + \Omega)}{\Omega T} \\ &\quad \text{Tr} \left[J_x^Q(\mathbf{k}) A(\mathbf{k}, \omega) J_x^Q(\mathbf{k}) A(\mathbf{k}, \omega + \Omega) \right], \end{aligned} \quad (11)$$

where n_F is the Fermi distribution function, $J_x^Q(\mathbf{k})$ is the matrix of heat current operator, $A(\mathbf{k}, \omega) = -\frac{1}{\pi} \text{Im} G^{\text{ret}}(\mathbf{k}, \omega) = \frac{\gamma}{(\omega - H^A(\mathbf{k}))^2 + \gamma^2}$ is the matrix of spectral function and we have added a small impurity scattering rate $\gamma = 0.03K_1$. Eq.(11) involves the derivative of n_F which is peaked at the Fermi energy with a width proportional to temperature T , hence only the states with energy close to the Fermi level within the scale of T can contribute to κ_{xx} . This indicates thermal conductivity will be small if the density of states near the Fermi energy is low.

The thermal conductivity as a function of h/K_1 for 0- and π -flux sectors with parameters $K_1 = 1, K_3 = 0.3, K'_3 = 0.34, T = \frac{1}{24}$ are plotted in Fig.3(a). We only show these two flux sectors because they have lower free energy than the other flux sectors, and the results for the other flux sectors are shown in the appendix. Fig.3(a) shows that the κ_{xx} curves develop dips and bumps as a function of magnetic field. The detailed shape of the curves depend on the parameters, but the appear-

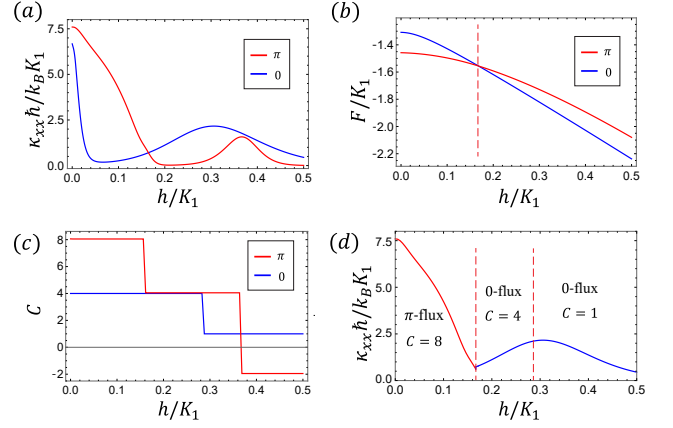


FIG. 3. Physical quantities as a function of h/K_1 for 0- and π -flux sectors with parameters $K_1 = 1, K_3 = 0.3, K'_3 = 0.34, T = \frac{1}{24}$. We only show the results for these two flux sectors because they have lower free energy than other flux sectors. (a) Thermal conductivity. (b) Free energy. (c) Chern number. (d) Thermal conductivity of the flux sector with the lowest free energy. The maxima of κ_{xx} in (a) coincide with the changes of Chern number in (c). The red dashed lines in (d) represent the transition from π - to 0-flux sector and the topological transition that changes Chern number. These transitions give rise to dip-bump features in thermal conductivity as a function of magnetic field.

ance of dip-bump features in each flux sector is generic. The free energy with the same parameters is shown in Fig.3(b). It shows the ground state is in the π -flux sector for small h and it goes through a transition to the 0-flux sector at large h . This first-order transition can lead to a jump in physical observables. Fig.3(d) shows the thermal conductivity of the flux sector with the lowest free energy. The red dashed line represents the phase transition from the π - to 0-flux sector, which is accompanied by a dip in κ_{xx} . The temperature dependence of thermal conductivity for 0- and π flux sectors are shown in Fig.4, where in (b) and (d) the curves are normalized by κ_{xx} at $h = 0$. It shows that the dips and bumps become weaker at low temperature, because thermal conductivity is a transport property at finite temperature which will decrease when temperature is low.

V. DIPS AND BUMPS IN THERMAL CONDUCTIVITY INDUCED BY PHASE TRANSITIONS

The dips and bumps of thermal conductivity as a function of magnetic field shown in Fig.3(a) and (d) is a generic feature that exists in a wide range in the parameter space. These phenomena can be understood from the transition between different flux sectors and the gap closing accompanied by the topological transitions that changes the Chern number. When the magnetic field is small, it tends to open a gap in the Majorana fermion bands for 0- and π -flux sectors. The low energy band structure $E(\mathbf{k})$ of 0- and π -flux sectors for the parameters in Fig.3(a) at zero and small h are shown in Fig.5. The spectrum at $h = 0$ without magnetic field is gapless for both flux

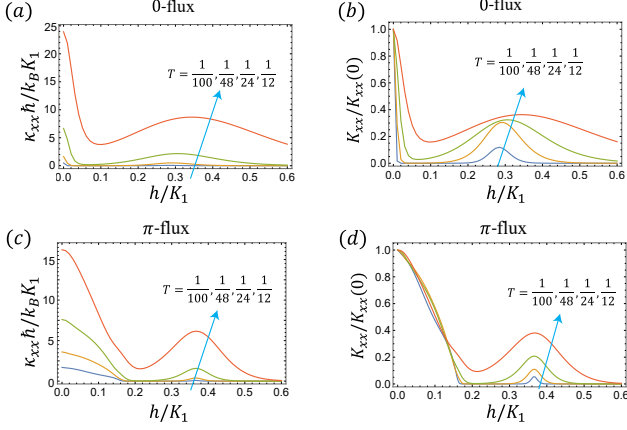


FIG. 4. Thermal conductivity as a function of h/K_1 for 0- and π -flux sectors at different temperature with $K_1 = 1, K_3 = 0.3, K'_3 = 0.34$. (a), (b) are for 0-flux sector and (c), (d) are for π -flux sector. (b) and (d) are rescaled by κ_{xx} at $h = 0$. The dips and bumps become weaker at low temperature.

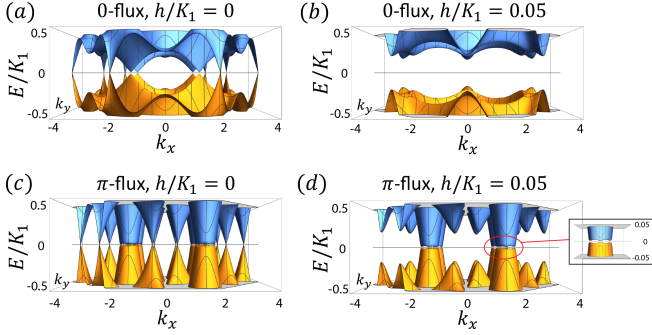


FIG. 5. Dispersion of Majorana bands near the Fermi energy for 0- and π -flux sectors with $K_1 = 1, K_3 = 0.3, K'_3 = 0.34$. For both flux sectors, the spectrum are gapless at $h = 0$, and a small h induced by magnetic field can open a gap. The gap in the π -flux sector is much smaller than that for the 0-flux sector.

sectors. When a small magnetic field is added, the spectrum in both flux sectors open a gap. From Eq.(11) the thermal conductivity is related to the density of states near the Fermi energy, therefore this gap reduces the thermal conductivity, leading to the decrease of κ_{xx} at small h for 0- and π -flux sectors in Fig.3(a).

When magnetic field increases, there is a transition from π - to 0-flux sector, which leads to a dip in thermal conductivity at $h/K_1 = 0.165$. As the magnetic field further increases, it can induce topological transitions that change the Chern number for the Majorana bands. The Chern number for each flux sector is shown in Fig.3(c), and a comparison with Fig.3(a) shows that the local maxima of thermal conductivity coincide with the change in Chern number. This is because the gap needs to close near transitions that change the Chern number, which leads to an increase in the density of states near Fermi energy. Because κ_{xx} is related to the density of state, this change in Chern number leads to an increase of κ_{xx} , which is the origin

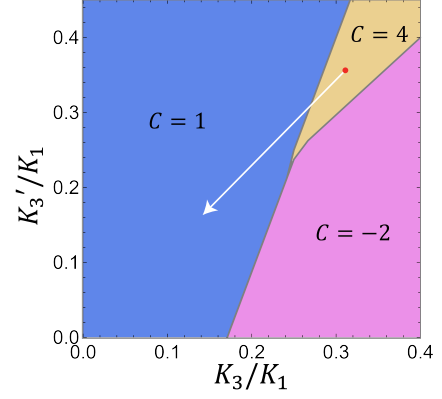


FIG. 6. Chern number of the 0-flux sector with finite H_2 and vanishing H_I . This phase diagram is independent of the magnitude of H_2 as long as H_2 is finite. Interaction H_I induced by the magnetic field can rescale the effective K_3 and K'_3 along the white arrow, leading to a phase transition that changes the Chern number.

of the bump of thermal conductivity near $h/K_1 = 0.3$.

The Majorana interaction term H_I induced by the magnetic field also plays an important role in the change of Chern number. Consider the 0-flux sector for simplicity in which all the Δ 's have the same value in the mean field solution. If we turn off interaction H_I but keep a finite H_2 (see Eq.(4)), the phase diagram of Chern number for the 0-flux sector with different K_3 and K'_3 is shown in Fig.6. From Eq.(7) the auxiliary field Δ modifies the NN hopping terms in the mean field Hamiltonian by changing K_1 to $K_1 + 2\Delta$. Because an overall scaling of Hamiltonian does not modify the Chern number, a system with parameters $\{K_1 + 2\Delta, K_3, K'_3\}$ has the same Chern number as the one with parameters $\{K_1, K_3 \frac{K_1}{K_1 + 2\Delta}, K'_3 \frac{K_1}{K_1 + 2\Delta}\}$. Therefore, the interaction term effectively rescales K_3 and K'_3 by a factor $\frac{K_1}{K_1 + 2\Delta}$. The mean field solution shows Δ is a positive number that grows with h . Therefore, if the system without magnetic field has K_3, K'_3 located at, e.g., the red dot in Fig.6, then as the magnetic field increases, h and Δ will increase and the effective K_3 and K'_3 will follow the white arrow in Fig.6. When the effective K_3 and K'_3 cross a phase boundary between different Chern numbers, the Chern number will change and the gap will close, leading to an increase in κ_{xx} . This explains the bump of κ_{xx} in the 0-flux sector in Fig.3(a) and (d) at $h/K_1 = 0.3$. As long as K_3 and K'_3 are chosen to be at $C = 4$ or $C = -2$ region close to the phase boundary, the bump in κ_{xx} is expected to occur, which is not sensitive to the exact choice of K_3 and K'_3 . Therefore, the change of Chern number induced by magnetic field is a robust feature of this Majorana system which is independent of the detailed parameter choice.

VI. DISCUSSIONS

We have shown that in quantum spin liquids an external magnetic field can induce dips and bumps in thermal conductivity κ_{xx} via phase transitions between different flux sectors

and different Chern numbers. It is tempting to compare our results to the recent experiments where oscillations of κ_{xx} with magnetic field was observed. The dip-bump features that we found in κ_{xx} become weaker at lower temperature, as shown in Fig.4, which could be consistent with the report in Ref 39 of a weakening trend of the oscillatory features at lower temperatures. Our model is a possible mechanism for the non-monotonic behavior in thermal conductivity, but it is difficult for a direct comparison between our model and realistic materials. Our model predicts the change in Chern number accompanies the local maxima of thermal conductivity, which will lead to a jump in thermal Hall conductivity κ_{xy} because κ_{xy} is related to Chern number, and this change in κ_{xy} will be sharper at lower temperature. The change of κ_{xy} near the bump of κ_{xx} has not been reported in candidate materials. The relation between κ_{xy} and the non-monotonic behavior of κ_{xx} are left as an open question for future investigation.

VII. ACKNOWLEDGMENT

This work is supported by the Natural Sciences and Engineering Research Council of Canada (NSERC) and the Center for Quantum Materials at the University of Toronto. H.Y.K acknowledges the support by the Canadian Institute for Advanced Research (CIFAR) and the Canada Research Chairs Program. Computations were performed on the Niagara supercomputer at the SciNet HPC Consortium. SciNet is funded by: the Canada Foundation for Innovation under the auspices of Com-

pute Canada; the Government of Ontario; Ontario Research Fund - Research Excellence; and the University of Toronto.

Appendix A: Thermal conductivity in other flux sectors

We have computed the thermal conductivity for various flux sectors including $0, \pi, \frac{1}{2}\pi, \frac{1}{3}\pi, \frac{2}{3}\pi, \frac{1}{4}\pi$, and $\frac{3}{4}\pi$. The plots for 0- and π -flux sectors are shown in the main text. Here we show the results for all these flux sectors in Fig.S1. The free energy for each flux sector as a function of h induced by magnetic field is plotted in Fig.S1(a). It shows the ground state with the lowest free energy is in 0- or π -flux sector. The thermal conductivity κ_{xx} is plotted in Fig.S1(b), which shows the dependence of κ_{xx} on magnetic field is non-monotonic in general within each flux sector. This non-monotonic behaviour is related to the change in Chern number as shown in Fig.S1(c). Within each flux sector, each local maximum of κ_{xx} coincides with a topological transition that changes the Chern number. This is because the change in Chern number accompanies the closure of Majorana band gap and an increase in density of states, which leads to increased thermal conductivity. Since the transitions that change the Chern number within each flux sector generically exist, and the transitions between different flux sectors driven by free energy can also lead to jumps in thermal conductivity, these transitions provide a generic mechanism to induce non-monotonic dependence of thermal conductivity on magnetic field.

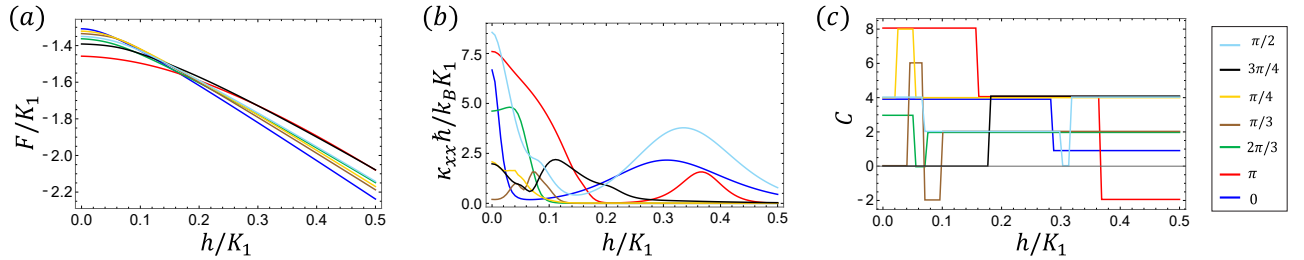


FIG. S1. Free energy (a), thermal conductivity (b) and Chern number (c) as a function of h induced by magnetic field for various flux sectors with $K_1 = 1, K_3 = 0.3, K'_3 = 0.34, T = \frac{1}{24}$. In (c) the overlapped curves are slightly shifted for better visibility.

* ybkim@physics.utoronto.ca

† hykee@physics.utoronto.ca

¹ P.W. Anderson, "Resonating valence bonds: A new kind of insulator?" *Materials Research Bulletin* **8**, 153–160 (1973).

² Xiao-Gang Wen, "Quantum orders and symmetric spin liquids," *Phys. Rev. B* **65**, 165113 (2002).

³ Leon Balents, "Spin liquids in frustrated magnets," *Nature* **464**, 199–208 (2010).

⁴ Lucile Savary and Leon Balents, "Quantum spin liquids: a review," *Reports on Progress in Physics* **80**, 016502 (2016).

⁵ Yi Zhou, Kazushi Kanoda, and Tai-Kai Ng, "Quantum spin liquid states," *Rev. Mod. Phys.* **89**, 025003 (2017).

⁶ M. Hermanns, I. Kimchi, and J. Knolle, "Physics of the kitaev model: Fractionalization, dynamic correlations, and material connections," *Annual Review of Condensed Matter Physics* **9**, 17–33 (2018).

- 7 J. Knolle and R. Moessner, “A field guide to spin liquids,” *Annual Review of Condensed Matter Physics* **10**, 451–472 (2019).
- 8 C. Broholm, R. J. Cava, S. A. Kivelson, D. G. Nocera, M. R. Norman, and T. Senthil, “Quantum spin liquids,” *Science* **367**, eaay0668 (2020).
- 9 Alexei Kitaev, “Anyons in an exactly solved model and beyond,” *Annals of Physics* **321**, 2–111 (2006), January Special Issue.
- 10 G. Jackeli and G. Khaliullin, “Mott insulators in the strong spin-orbit coupling limit: From heisenberg to a quantum compass and kitaev models,” *Phys. Rev. Lett.* **102**, 017205 (2009).
- 11 Jeffrey G. Rau, Eric Kin-Ho Lee, and Hae-Young Kee, “Generic spin model for the honeycomb iridates beyond the kitaev limit,” *Phys. Rev. Lett.* **112**, 077204 (2014).
- 12 Jeffrey G. Rau and Hae-Young Kee, “Trigonal distortion in the honeycomb iridates: Proximity of zigzag and spiral phases in Na_2IrO_3 ,” (2014), [arXiv:1408.4811](#).
- 13 Jeffrey G. Rau, Eric Kin-Ho Lee, and Hae-Young Kee, “Spin-orbit physics giving rise to novel phases in correlated systems: Iridates and related materials,” *Annual Review of Condensed Matter Physics* **7**, 195–221 (2016).
- 14 Simon Trebst, “Kitaev materials,” (2017), [arXiv:1701.07056](#).
- 15 Y. Kasahara, T. Ohnishi, Y. Mizukami, O. Tanaka, Sixiao Ma, K. Sugii, N. Kurita, H. Tanaka, J. Nasu, Y. Motome, T. Shibauchi, and Y. Matsuda, “Majorana quantization and half-integer thermal quantum hall effect in a kitaev spin liquid,” *Nature* **559**, 227–231 (2018).
- 16 Matthias Gohlke, Gideon Wachtel, Youhei Yamaji, Frank Pollmann, and Yong Baek Kim, “Quantum spin liquid signatures in kitaev-like frustrated magnets,” *Phys. Rev. B* **97**, 075126 (2018).
- 17 Hidenori Takagi, Tomohiro Takayama, George Jackeli, Giniyat Khaliullin, and Stephen E. Nagler, “Concept and realization of kitaev quantum spin liquids,” *Nature Reviews Physics* **1**, 264–280 (2019).
- 18 Yukitoshi Motome and Joji Nasu, “Hunting majorana fermions in kitaev magnets,” *Journal of the Physical Society of Japan* **89**, 012002 (2020).
- 19 Mengxing Ye, Rafael M. Fernandes, and Natalia B. Perkins, “Phonon dynamics in the kitaev spin liquid,” *Phys. Rev. Research* **2**, 033180 (2020).
- 20 Jean-Noël Fuchs, Sourabh Patil, and Julien Vidal, “Parity of chern numbers in the kitaev honeycomb model and the sixteenfold way,” *Phys. Rev. B* **102**, 115130 (2020).
- 21 Shaozhi Li and Satoshi Okamoto, “Thermal hall effect in the kitaev-heisenberg system with spin-phonon coupling,” (2021), [arXiv:2112.06107](#).
- 22 Kexin Feng, Mengxing Ye, and Natalia B. Perkins, “Temperature evolution of the phonon dynamics in the kitaev spin liquid,” *Phys. Rev. B* **103**, 214416 (2021).
- 23 Yogesh Singh and P. Gegenwart, “Antiferromagnetic mott insulating state in single crystals of the honeycomb lattice material Na_2IrO_3 ,” *Phys. Rev. B* **82**, 064412 (2010).
- 24 Jiří Chaloupka, George Jackeli, and Giniyat Khaliullin, “Kitaev-heisenberg model on a honeycomb lattice: Possible exotic phases in iridium oxides A_2IrO_3 ,” *Phys. Rev. Lett.* **105**, 027204 (2010).
- 25 X. Liu, T. Berlijn, W.-G. Yin, W. Ku, A. Tsvelik, Young-June Kim, H. Gretarsson, Yogesh Singh, P. Gegenwart, and J. P. Hill, “Long-range magnetic ordering in Na_2IrO_3 ,” *Phys. Rev. B* **83**, 220403 (2011).
- 26 Yogesh Singh, S. Manni, J. Reuther, T. Berlijn, R. Thomale, W. Ku, S. Trebst, and P. Gegenwart, “Relevance of the heisenberg-kitaev model for the honeycomb lattice iridates A_2IrO_3 ,” *Phys. Rev. Lett.* **108**, 127203 (2012).
- 27 S. K. Choi, R. Coldea, A. N. Kolmogorov, T. Lancaster, I. I. Mazin, S. J. Blundell, P. G. Radaelli, Yogesh Singh, P. Gegenwart, K. R. Choi, S.-W. Cheong, P. J. Baker, C. Stock, and J. Taylor, “Spin waves and revised crystal structure of honeycomb iridate Na_2IrO_3 ,” *Phys. Rev. Lett.* **108**, 127204 (2012).
- 28 K. A. Modic, Tess E. Smidt, Itamar Kimchi, Nicholas P. Breznay, Alun Biffin, Sungkyun Choi, Roger D. Johnson, Radu Coldea, Pilanda Watkins-Curry, Gregory T. McCandless, Julia Y. Chan, Felipe Gandara, Z. Islam, Ashvin Vishwanath, Arkady Shekhter, Ross D. McDonald, and James G. Analytis, “Realization of a three-dimensional spin-anisotropic harmonic honeycomb iridate,” *Nature Communications* **5**, 4203 (2014).
- 29 Heung-Sik Kim, Yong Baek Kim, and Hae-Young Kee, “Revealing frustrated local moment model for pressurized hyperhoneycomb iridate: Paving the way toward a quantum spin liquid,” *Phys. Rev. B* **94**, 245127 (2016).
- 30 K. W. Plumb, J. P. Clancy, L. J. Sandilands, V. Vijay Shankar, Y. F. Hu, K. S. Burch, Hae-Young Kee, and Young-June Kim, “ $\alpha - \text{ruCl}_3$: A spin-orbit assisted mott insulator on a honeycomb lattice,” *Phys. Rev. B* **90**, 041112 (2014).
- 31 Luke J. Sandilands, Yao Tian, Kemp W. Plumb, Young-June Kim, and Kenneth S. Burch, “Scattering continuum and possible fractionalized excitations in $\alpha - \text{ruCl}_3$,” *Phys. Rev. Lett.* **114**, 147201 (2015).
- 32 Heung-Sik Kim, Vijay Shankar V., Andrei Catuneanu, and Hae-Young Kee, “Kitaev magnetism in honeycomb ruCl_3 with intermediate spin-orbit coupling,” *Phys. Rev. B* **91**, 241110 (2015).
- 33 J. A. Sears, M. Songvilay, K. W. Plumb, J. P. Clancy, Y. Qiu, Y. Zhao, D. Parshall, and Young-June Kim, “Magnetic order in $\alpha - \text{ruCl}_3$: A honeycomb-lattice quantum magnet with strong spin-orbit coupling,” *Phys. Rev. B* **91**, 144420 (2015).
- 34 M. Majumder, M. Schmidt, H. Rosner, A. A. Tsirlin, H. Yasuoka, and M. Baenitz, “Anisotropic $\text{ru}^{3+}4d^5$ magnetism in the $\alpha - \text{ruCl}_3$ honeycomb system: Susceptibility, specific heat, and zero-field nmr,” *Phys. Rev. B* **91**, 180401 (2015).
- 35 Luke J. Sandilands, Yao Tian, Anjan A. Reijnders, Heung-Sik Kim, K. W. Plumb, Young-June Kim, Hae-Young Kee, and Kenneth S. Burch, “Spin-orbit excitations and electronic structure of the putative kitaev magnet $\alpha - \text{ruCl}_3$,” *Phys. Rev. B* **93**, 075144 (2016).
- 36 A. Banerjee, C. A. Bridges, J.-Q. Yan, A. A. Aczel, L. Li, M. B. Stone, G. E. Granroth, M. D. Lumsden, Y. Yiu, J. Knolle, S. Bhat-tacharjee, D. L. Kovrizhin, R. Moessner, D. A. Tennant, D. G. Mandrus, and S. E. Nagler, “Proximate kitaev quantum spin liquid behaviour in a honeycomb magnet,” *Nature Materials* **15**, 733–740 (2016).
- 37 Seung-Hwan Do, Sang-Youn Park, Junki Yoshitake, Joji Nasu, Yukitoshi Motome, Yong Seung Kwon, D. T. Adroja, D. J. Voneshen, Kyoo Kim, T.-H. Jang, J.-H. Park, Kwang-Yong Choi, and Sungdae Ji, “Majorana fermions in the kitaev quantum spin system $\alpha - \text{ruCl}_3$,” *Nature Physics* **13**, 1079–1084 (2017).
- 38 Daichi Hirobe, Masahiro Sato, Yuki Shiomi, Hidekazu Tanaka, and Eiji Saitoh, “Magnetic thermal conductivity far above the néel temperature in the kitaev-magnet candidate $\alpha - \text{ruCl}_3$,” *Phys. Rev. B* **95**, 241112 (2017).
- 39 Peter Czajka, Tong Gao, Max Hirschberger, Paula Lampen-Kelley, Arnab Banerjee, Jiaqiang Yan, David G. Mandrus, Stephen E. Nagler, and N. P. Ong, “Oscillations of the thermal conductivity in the spin-liquid state of $\alpha - \text{ruCl}_3$,” *Nature Physics* **17**, 915–919 (2021).
- 40 J. A. N. Bruin, R. R. Claus, Y. Matsumoto, N. Kurita, H. Tanaka, and H. Takagi, “Robustness of the thermal hall effect close to half-quantization in a field-induced spin liquid state,” (2021), [arXiv:2104.12184](#).
- 41 S. Suetsugu, Y. Ukai, M. Shimomura, M. Kamimura, T. Asaba, Y. Kasahara, N. Kurita, H. Tanaka, T. Shibauchi, J. Nasu, Y. Mo-

- tome, and Y. Matsuda, “Evidence for the first-order topological phase transition in a kitaev spin liquid candidate α -rucl₃,” (2022), [arXiv:2203.00275](#).
- ⁴² Shang-Shun Zhang, Zhentao Wang, Gábor B. Halász, and Cristian D. Batista, “Vison crystals in an extended kitaev model on the honeycomb lattice,” *Phys. Rev. Lett.* **123**, 057201 (2019).
- ⁴³ Shang-Shun Zhang, Cristian D. Batista, and Gábor B. Halász, “Toward kitaev’s sixteenfold way in a honeycomb lattice model,” *Phys. Rev. Research* **2**, 023334 (2020).
- ⁴⁴ Elliott H. Lieb, “Flux phase of the half-filled band,” *Phys. Rev. Lett.* **73**, 2158–2161 (1994).
- ⁴⁵ Chengshu Li and Marcel Franz, “Majorana-hubbard model on the honeycomb lattice,” *Phys. Rev. B* **98**, 115123 (2018).
- ⁴⁶ Hosho Katsura, Naoto Nagaosa, and Patrick A. Lee, “Theory of the thermal hall effect in quantum magnets,” *Phys. Rev. Lett.* **104**, 066403 (2010).
- ⁴⁷ Gerald D Mahan, *Many-particle physics* (Springer Science & Business Media, 2013).
- ⁴⁸ Adam C. Durst and Patrick A. Lee, “Impurity-induced quasiparticle transport and universal-limit wiedemann-franz violation in d-wave superconductors,” *Phys. Rev. B* **62**, 1270–1290 (2000).
- ⁴⁹ Wen O. Wang, Jixun K. Ding, Brian Moritz, Edwin W. Huang, and Thomas P. Devereaux, “Magnon heat transport in a 2d mott insulator,” (2021), [arXiv:2109.01119](#).